VLA hydrogen and helium 76-alpha line observations of Sagittarius B2

Roelsema, PR; Goss, WM; Whiteoak, JB; Gardner, FF; Pankonin, V.

Published in:
Astronomy & astrophysics

Publication date:
1987

Astron. Astrophys. 175, 219–230 (1987)

ASTRONOMY
AND
ASTROPHYSICS

VLA hydrogen and helium 76 α line observations of Sagittarius B2

P.R. Roelfsema [1], W.M. Goss [1,2], J.B. Whiteoak [3], F.F. Gardner [3], and V. Pankonin [4]

[1] Kapteyn Astronomical Institute, Postbus 800, 9700 AV Groningen, The Netherlands
[2] NRAO, VLA, Socorro, NM 87801, USA
[3] Division of Radiophysics, CSIRO, P.O. Box 76, Epping, NSW 2121, Australia
[4] National Science Foundation, Washington, D.C., USA

Received May 5, accepted Dezember 3, 1986

Summary. The H II region complex Sgr B2 (G0.7–0.0) has been mapped with the Very Large Array (VLA) with an angular resolution of $3''.8 \times 3''.4\,(\alpha \times \delta)$ and a velocity resolution of $8\,\mathrm{km\,s^{-1}}$. The distribution of the H 76α and He 76α line emission has been determined over the 11 continuum components of this complex. The observations are consistent with a $y^+ = [He^+]/[H^+]$ of ~10% in 10 of the 11 compact components. The effects of an appreciable continuum optical depth near the compact components in G0.7S are apparent in a decrease in the line to continuum ratio of the hydrogen line. The quantity y^+ shows an increase with distance from the centre of the compact components. This trend is caused by two effects: (1) near the most compact components in G0.7S the helium ionized zone is smaller than that of hydrogen leading to an apparently weak helium line and (2) in the surrounding components the helium and hydrogen ionized volumes are comparable. In the direction of G0.7N at least three velocity systems are observed, two of which have counterparts in the surrounding molecular cloud.

Key words: nebulae – H II regions – radio lines

1. Introduction

The galactic H II region Sagittarius B2 (G0.7–0.0 or W24) is one of the most spectacular nebulae in our galaxy. This totally obscured H II region has been the subject of numerous radio and infrared studies and the associated molecular cloud is the source of many exotic molecular lines.

There have been many radio recombination studies with single dish radio telescopes of Sgr B2 with angular resolutions ranging from ~1′ to 6′. Garay et al. (1985) have presented VLA data of the H 76α line at 14.7 GHz of two of the components of Sgr B2. On the basis of ~5″ resolution H 76α observations Garay (1985) concluded that a south-north gradient of $\sim 10\,\mathrm{km\,s^{-1}}$/arcmin is present in the velocities of the H II regions in Sgr B2. Garay explained this gradient qualitatively in terms of a collapsing molecular cloud. This molecular cloud would have a flattened core of ~3 pc at the centre of Sgr B2 and would be rotating with an angular velocity of $\sim 10^{-13}\,\mathrm{s^{-1}}$. The cloud is then contracting with velocities of $\sim 10\,\mathrm{km\,s^{-1}}$. Fragmentation of the molecular cloud could then lead to multiple sites of star formation at the observed velocities. A vast literature has developed concerning the problem of the helium abundance in Sgr B2. Churchwell and Mezger (1973) found an apparent ionized helium to hydrogen ratio ($y^+ = [He^+]/[H^+]$) < 2% at 5 GHz, while later authors found a y^+ of ~9% at 14.7 GHz. Recent interpretations of the low values of y^+ have concentrated on 1) preferential absorption of He ionizing photons due to dust in the H II region (e.g. Mezger and Smith, 1976; Chaisson et al., 1978), 2) non-LTE processes in a cold, partially ionized region exterior to Sgr B2 (Brown and Lockman, 1975) giving rise to an enhancement of the hydrogen line and 3) a multi-component model (core-halo) with pressure broadening and an intrinsic $y = [He]/[H] = 10\%$ (Pitault and Cesarsky, 1980).

In this paper we present H 76α and He 76α observations of the Sgr B2 complex with a resolution of ~4″. The major goals have been: (1) a determination of the physical parameters of the individual H II components, in particular a determination of variations in y^+, and (2) possible changes of the H II parameters over the extended components.

2. Observations

The observational parameters are summarized in Table 1. We used the C-D array of the VLA of the National Radio Astronomy Observatory [1] with the north arm in the C array configuration and the south-east and south-west arms in the D array configuration. Thus, a circular beam at a declination of −28° is possible. The velocity was centred at $20\,\mathrm{km\,s^{-1}}$ in order to include both the H 76α and He 76α lines in the 12.5 MHz ($255\,\mathrm{km\,s^{-1}}$) band; the velocity separation of the H and He lines is $122.0\,\mathrm{km\,s^{-1}}$. The relative gains and phases within each band were determined using 3C84. The data were calibrated, edited and Fourier transformed using the standard VLA calibration and reduction software. All post-map processing was done using the Groningen Image Processing System (GIPSY; Allen et al., 1985).

Send offprint requests to: P.R. Roelfsema

[1] Operated by Associated Universities Inc., under contract with the National Science Foundation

Table 1. VLA instrumental parameters

Source	Sagittarius B2
Field centre	$\alpha(1950) = 17^h44^m10^s.50$
	$\delta(1950) = -28°21'35''.0$
Date of observation	5–6 July, 1984
Total time (h)	8
Number of telescopes	25
Configuration	C-D
Baseline (km)	Minimum Maximum
	0.04 11.4
Polarization	Right circular
Flux density calibrator	1741–312
Flux density (Jy)	0.38
Bandpass calibrator	3C84
Flux density (Jy)	51.4 Jy
Rest frequency (MHz)	14689.990
Total bandwidth (MHz)	12.5 (255 km s^{-1})
Number of velocity channels	31
Central velocity (channel 16) (km s^{-1})	20
Channel separation (km s^{-1})	7.97
Velocity resolution (km s^{-1})	7.97
Synthesized beam	$3''.8 \times 3''.4$ ($\alpha \times \delta$)
T_b/S (K/mJy beam^{-1})	0.4
rms in line maps (mJy beam^{-1})	2.5
rms in continuum map (mJy beam^{-1})	13

3. Results

3.1. Continuum

In Fig. 1 we show the "cleaned" (Högbom, 1974) continuum map of Sgr B2 at 14.7 GHz with a resolution of $3''.8 \times 3''.4$ ($\alpha \times \delta$). This map was made by averaging six of the line free channels. It was not corrected for primary beam attenuation. Previous high resolution VLA maps of Sgr B2 have been published by Benson and Johnston (1984) with resolutions of about 1″ at 15 GHz and 2″.7 at 4.9 GHz. The 12 components found in these higher resolution maps (their components A to L) are shown as crosses in Fig. 1. The total flux density in this map is 20 ± 1 Jy as compared to single dish values of 33 Jy near 15 GHz (Hobbs and Johnston, 1971); thus only about 60 % of the total flux density is detected by the VLA at this resolution. The higher resolution map of Benson and Johnston (1984) misses ~50 % of the total flux density. On the basis of the continuum morphology we divided the complex into 11 components to be used separately in our analysis. These components are also indicated in the map, with a summary of their continuum parameters (corrected for primary beam attentuation) in Table 2. Continuum components 7, 8, 9 (component K of Benson and Johnston) refer to the south-west quarter, south-east quarter and northern-half, respectively (Fig. 1). The component 3 shown in Fig. 1 consists of six components in the Benson and Johnston map (B, D, E, F, G and I). The shell source I is the dominant component (67 % of the total flux density) and its position coincides with the peak of our component 3. Component F to the north west of I is the second dominant component with 20 % of the total flux density.

3.2. Line

For each pixel a single linear baseline was fitted to the maps containing no line emission (velocities −92 to −84, −20 to +4, and +116 to +132 km s^{-1}) and subtracted from all channels. Thus maps containing only line emission were obtained. These "dirty" maps were then "cleaned" in the usual manner. The rms noise of the line channels is more favourable than that of the continuum. The noise of the latter map is increased by instrumental effects, resulting in a dynamic range of ~200:1. For each of the 11 components shown in Fig. 1, total 76 α profiles were obtained by integrating the signal in every channel over the area where the component has a continuum brightness higher than 50 mJy beam^{-1}. These profiles are shown in Fig. 2a–l. Figure 2a is the total profile for all components; this profile represents the average profile for the small scale structure in Sgr B2. To each of these profiles a single, or in the presence of a helium line, a double Gaussian was fitted using a least squares fitting algorithm. The fitted Gaussians were accepted as a good model for the profiles only if all free parameters had a formal signal to noise ratio better than three. Furthermore helium line fits were only accepted if the resulting velocity was within 3σ of the velocity of the hydrogen line in the same profile. Since a *single* linear baseline had already been subtracted from the data the problem of underestimating line

Table 2. Continuum parameters of Sgr B2 sources

Number	α (1950)	δ (1950)	Total flux density (Jy)	Peak flux density (Jy)	Source size (arcsec)
1	$17^h44^m10^s.60$	$-28°22'42''.7$	0.81	0.55	2.1
2	17 44 10.2	−28 22 13	0.23	0.14	4
3	17 44 10.59	−28 22 03″.1	7.4	2.0	4.5
4	17 44 09.6	−28 21 58	1.5	0.45	5.4
5	17 44 10.7	−28 21 54	1.2	0.38	5.2
6	17 44 09.0	−28 21 44	0.57	0.16	7
7–9	17 44 10.6	−28 21 12	7.5	0.66	11
10	17 44 12.90	−28 20 53″.3	1.1	0.51	3.5
11	17 44 16.5	−28 21 02	1.3	0.18	8.8

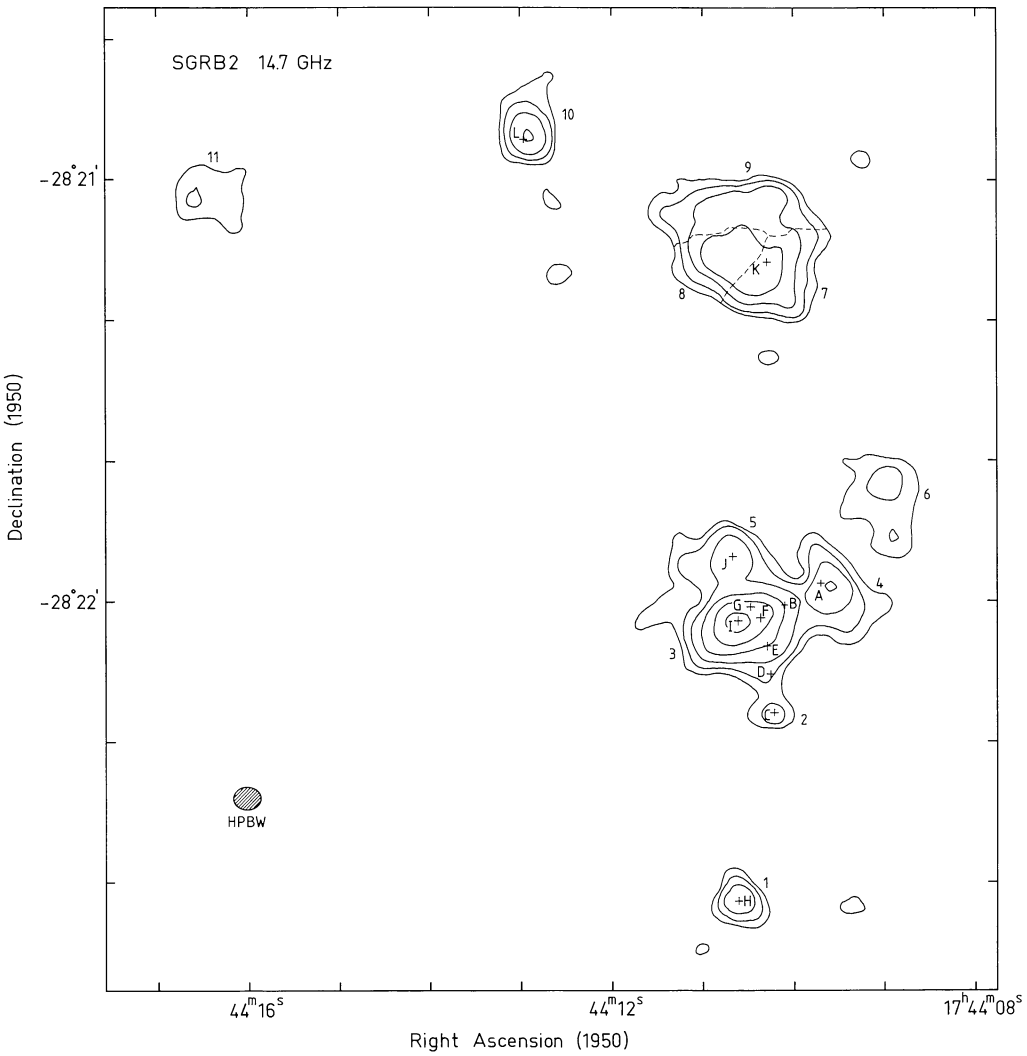

Fig. 1. Continuum map of Sgr B2 at 14.7 GHz with an angular resolution of 3″.8 × 3″.4 ($\alpha \times \delta$). This map was made by averaging six of the channels which contain no line emission. The numbers indicate the sources for which integrated profiles (Fig. 2) have been created. The source G0.7 N has been divided into three components: 7, 8, 9. These are indicated by dotted lines. The crosses are the locations of the 12 components observed by Benson and Johnston (1984) with a resolution of ~1″ (their components A–L). The contour units are 50, 100, 200, 400, 800, and 1600 mJy beam^{-1}. The rms noise is 13 mJy beam^{-1} and is limited by a dynamic range of ~22 db. This map is not corrected for primary beam attenuation

flux densities because of piecewise removal of a baseline as suggested by Pitault and Cesarsky (1980) does not occur. The model fits and one sigma errors (below each parameter in parentheses) are listed in Table 3. The parameters for the hydrogen lines are given in columns 2–5. The LTE electron temperature (T_e*) derived from the H 76α parameters (Brown, 1980, Eq. 2) are listed in column 5; we have assumed that the continuum optical depth is much less than one (see Sect. 4). The helium parameters are listed in columns 6–8. The apparent singly ionized helium abundance y^+ is based on the ratio of the line integrals and is listed in column 8.

To facilitate comparisons with single dish data, the average over all components, the average of 7, 8, 9 (G0.7N) and the average of 2, 3, 4, 5, 6 (G0.7S) are listed at the end of the table. The parameters of the mean profile (Fig. 2a) are in reasonable agreement with the 65α data (H and He) of Chaisson et al. (1978) taken with a beam width of 1′.2. The current data for G0.7S (average 2, 3, 4, 5, 6) are in reasonable agreement with the 76α data of Thum et al. (1978) taken with the 100 m telescope and a beam width of 55″. The major exception is the width of the He 76α line; our data gives 19.1 ± 4.1 km s^{-1}, in contrast to the 100 m telescope data, 44.4 ± 5.8 km s^{-1}. The Effelsberg 100 m data at 66α obtained by Thum (private communication) with a 45″ beam of G0.7N and G0.7S are also listed at the end of Table 3; the agreement with our data is excellent. The data of Garay et al. (1985) for component 3 (their Sgr B2M) are in excellent agreement and for component 1 (their Sgr B2S) in reasonable agreement. (The line width measured here of 65.2 ± 6.3 km s^{-1} is considerably broader than the value of 37.2 ± 1.4 km s^{-1} observed by Garay et al.). The H 76α line parameters of components 1 through 10 as observed here also agree to within the combined errors with those reported by Garay (1985).

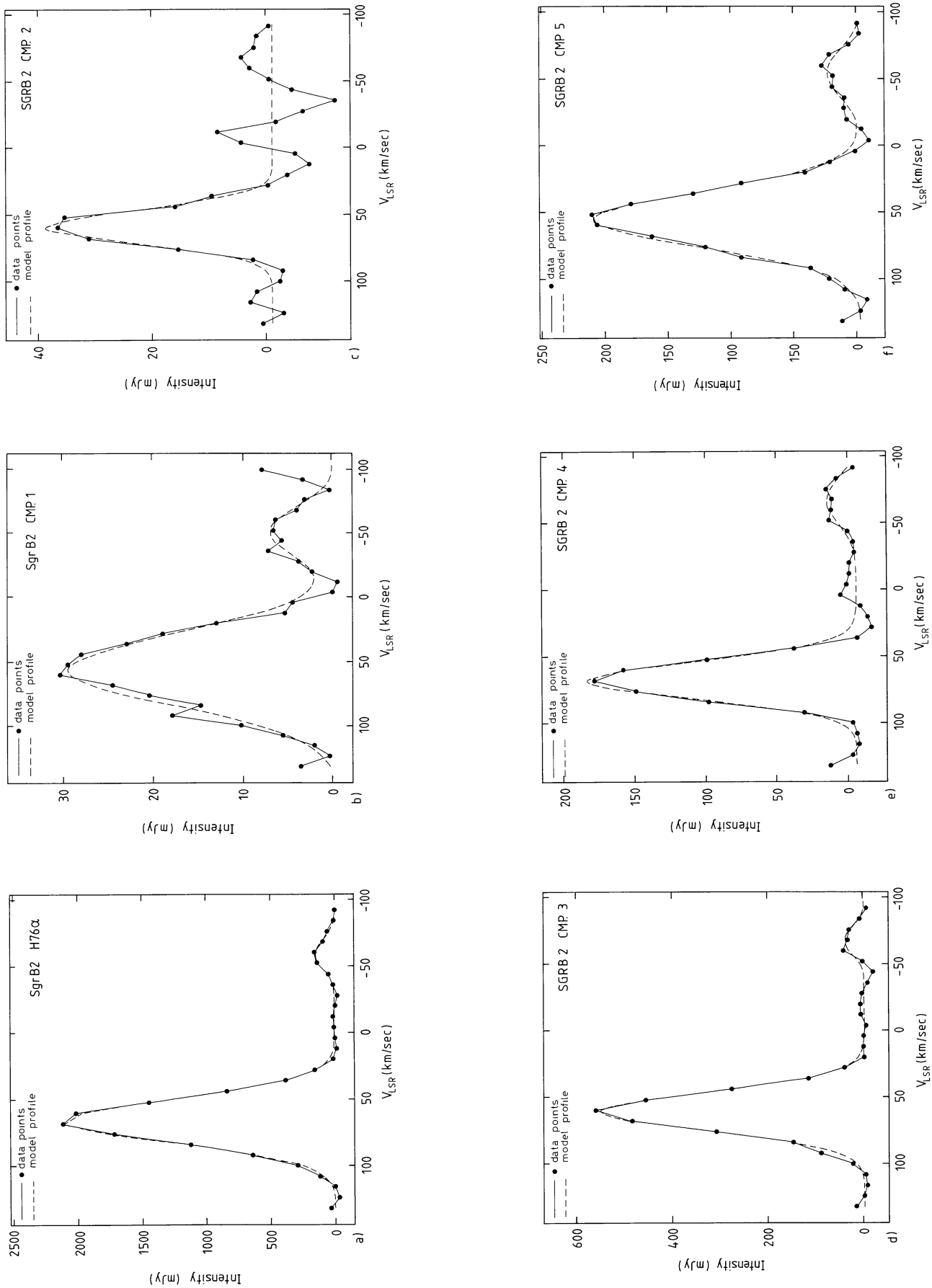

Fig. 2a–l. Mean profiles of the H and He 76α lines in the direction of **a** average of all components of Sgr B2, and **b** to **l** individual components of Sgr B2 (see Fig. 1). The velocity scale (LSR) is with respect to the hydrogen line and the helium velocity scale is obtained by adding 122.5 kms^{-1} to the hydrogen velocity. The data (solid line) and model gaussian fit (dashed) are shown

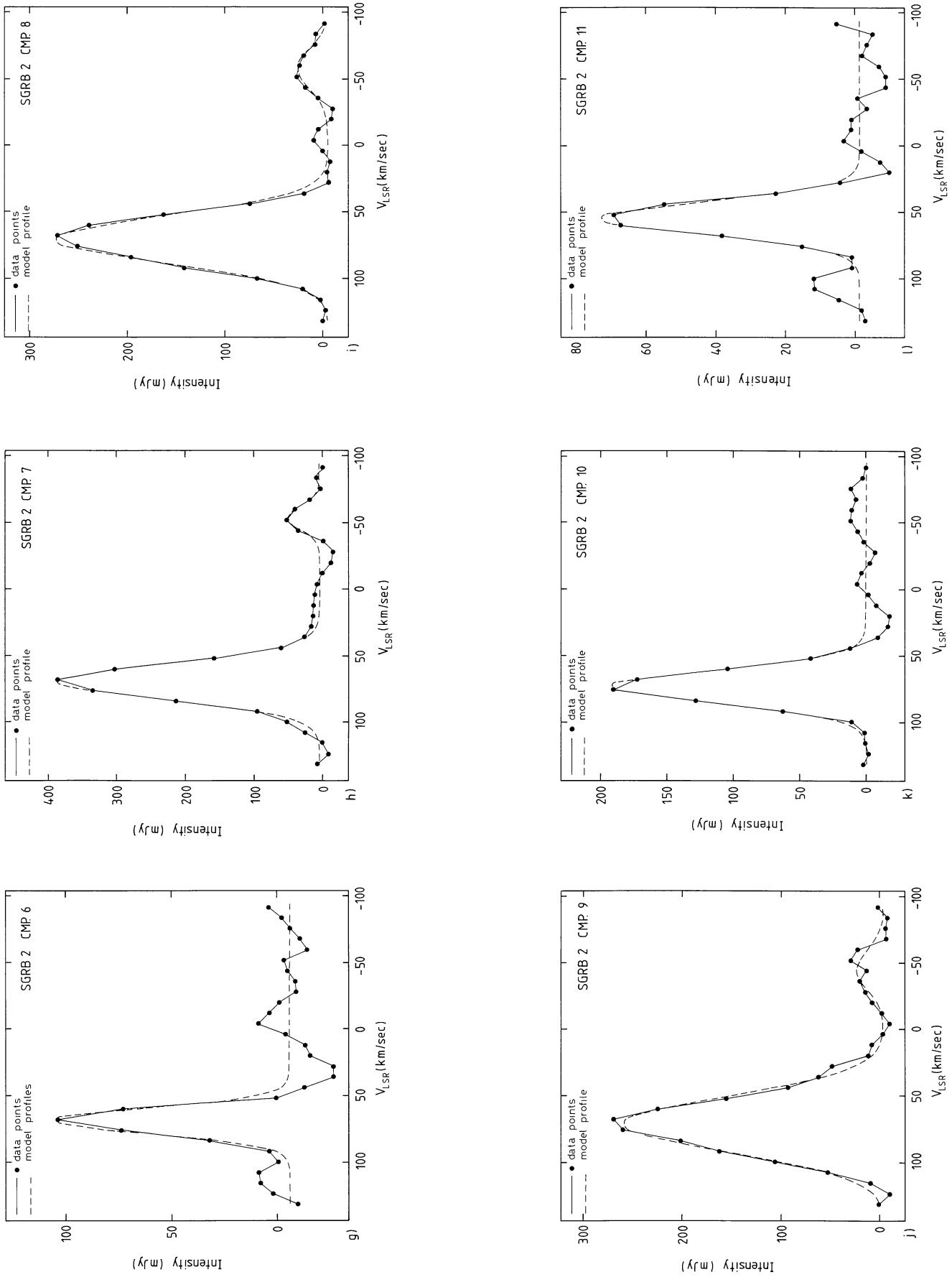

Fig. 2g–l (continued)

Table 3. 76α integral profiles in Sgr B2

Number	H				He		y^+
	V	ΔV	L/C	T_e	V	ΔV	
	($km\,s^{-1}$)		(%)	(K)	($km\,s^{-1}$)		(%)
1	56.1 (1.2)	65.2 (6.3)	10	5900 (1000)	72 (4)	44 (17)	17 (10)
2	58.8 (1.2)	29.2 (3.0)	17	6700 (650)	–	–	<20
3	60.3 (0.2)	33.8 (0.6)	8	11450 (500)	56 (3)	20 (6)	4.7 (1.4)
4	67.5 (0.5)	32.1 (1.2)	13	7750 (300)	56 (4)	38 (13)	12.8 (4.5)
5	55.2 (0.5)	48.6 (1.5)	16	4550 (180)	68 (3)	40 (14)	11 (3)
6	69.0 (0.8)	21.7 (2.0)	14	10100 (900)	–	–	<20
7	69.4 (0.3)	31.5 (0.8)	15	6800 (200)	69 (2)	19 (4)	8.1 (1.8)
8	70.5 (0.4)	40.8 (1.1)	11	7000 (200)	65 (3)	34 (9)	9.4 (2.6)
9	71.3 (0.5)	48.2 (1.7)	11	6100 (400)	78 (4)	34 (13)	7.7 (3.4)
10	73.2 (0.4)	28.3 (1.0)	19	6200 (400)	–	–	<10
11	54.2 (0.8)	28.5 (2.0)	14	8100 (600)	–	–	<20
A11	65.9 (0.1)	38.5 (0.4)	10	8000 (300)	64 (2)	24 (4)	4.7 (0.8)
7–9 G0.7N	70.1 (0.3)	38.9 (1.0)	13	6600 (500)	69 (1)	27 (2)	8.3 (0.8)
G0.7N[a]	69.9 (0.2)	36.9 (0.4)		6700 (300)	66.2 (1.6)	25 (4)	5.5 (1.2)
2–6 G0.7S	61.5 (0.2)	36.2 (0.4)	13	10400 (400)	59 (2)	19 (4)	3.9 (0.8)
G0.7S[a]	62.8 (0.3)	38.5 (0.6)		7800 (300)	57.7 (2.4)	28 (6)	6.8 (2.0)

[a] 100 m data at 66α (Thum, private communication)

4. Discussion

4.1. Pressure broadening

The determination of electron temperatures (Sect. 3) is based on the assumption of no pressure broadening. Since the rms densities of the six compact components in component 3 are known, using the data of Benson and Johnston (1984) it is possible to calculate the effects of pressure broadening. Using Eq. (3) of Garay et al. we may estimate the ratio of total line width (ΔV_T) to thermal line width (ΔV_{Th}). Within the 3.″8 × 3.″4 beam the mean rms $n_{e,rms}$ based on the Benson and Johnston (1984) data is $\sim 8\ 10^4\ cm^{-3}$. The relevant density for pressure broadening is, of course, the local density which is $f^{-1/2} \times n_{e,rms}$ where f is the filling factor. Based on the results of Pitault and Cesarsky (1980) we estimate that the filling factor must be >0.1. With this limit for $n_{e,true} < 2.5\ 10^5\ cm^{-3}$, the ratio $\Delta V_T/\Delta V_{Th} < 1.15$. Thus, it appears that pressure broadening is essentially negligible for the conditions in the compact sources in component 3.

4.2. Line to continuum ratio

For most of the components in Sgr B2 the line to continuum ratio (L/C) is ~10–15 %. For example for component 7, L/C is 15 %,

for component 6, 14%, and for the average of all components of Sgr B2, the L/C is 10%.

The mean L/C for component 3 is 7.7 ± 0.2% and the derived electron temperature of $11{,}450 \pm 220$ K is the highest for all of the 11 components in Sgr B2. However there is considerable variation in L/C near component 3. To the east of 3 (at the peak L/C = 8%) the L/C is in the range 11–13% while to the west in the direction of the compact component F ($EM = 2.6\ 10^9\ \mathrm{cm}^{-6}$ pc, $n_{e,\mathrm{rms}} = 1.9\ 10^5\ \mathrm{cm}^{-3}$) the L/C decreases rapidly to ~2–3%.

Based on the Benson and Johnston (1984) observations it is possible to calculate the mean continuum optical depth in component 3. Within the six components that make up component 3, a mean value of the emission measure (EM) is $\sim 5\ 10^8\ \mathrm{cm}^{-6}$ pc. The implied continuum opacity, τ_c at 14.7 GHz is then ~0.8 and the correction factor for the electron temperature $[\tau_c/(e^{\tau_c}-1)]^{0.87} = 0.69$. The T_e of 11,450 (Table 3) then becomes ~8000 K, in better agreement with the other components in Sgr B2. In the direction of component F the continuum opacity approaches ~2–3 and the L/C ratio is reduced by a factor $[\tau_c/(e^{\tau_c}-1)] = 0.3 - 0.16$, in good agreement with the observations.

By observing this source in higher frequency recombination lines it should be possible to obtain more detailed information about the electron temperature of the different sources comprising our component 3. At higher frequencies a higher resolution can be obtained and, more important, the continuum opacity will be less. Thus the line emission will be attenuated then allowing a more accurate determination of T_e.

4.3. Helium abundances

The abundance of ionized helium (y^+) was calculated for all components by dividing the fitted He 76α line intensities by those of the H 76α line. These values, or three σ upper limits for the abundance, that for *all* components in Sgr B2 except component 3, the data are consistent with a y^+ in the range 8–10%. For component 3 the y^+ is 4.7 ± 1.4%. Thus as Thum et al. (1978) have proposed it is clear that structural properties in Sgr B2 can account for the previously observed variations in the ionized helium abundance. At lower frequencies with lower resolution (see Thum et al.) the radiation is dominated by the large scale low density envelope (not observed in the current observations) with a y^+ in the range 3–4%.

Only in the directions of the component 3 and 7-8-9 are the signal to noise ratios in the helium line sufficient to look for possible variations in y^+ within the source itself. In the direction of 7-8-9 the mean value of y^+ is 8.3 ± 0.8%. There are no significant variations of y^+ over this component.

In component 3, there do appear to be significant variations in y^+ over the source. The value of y^+ near the centre of component 3 was found to be only 2.8 ± 0.7% (see Fig. 3a), significantly lower than that in the other components. To obtain a measure for radial varations of y^+ near component 3 the line data were integrated over concentric rings centred on the peak of component 3 (defined to be $\alpha(1950) = 17^h44^m10^s.6$, $\delta(1950) = -28°22'03''$) with widths of 1–2″. The line intensity per pixel drops rapidly with radius but the number of pixels per ring increases with radius and thus after integration over the rings, profiles with reasonable signal to noise ratio are obtained for all radii. For all these ring-integrated profiles a Gaussian component could be fitted to both the H 76α line and the He 76α line. The parameters of the fitted Gaussians are given in Table 4. Also given are the estimated 1σ errors. From the Gaussian parameters the LTE electron temperature T_e^* and the apparent abundance of singly ionized helium y^+ were calculated. In Fig. 3 two profiles obtained in this way are shown: the profile near the centre of component 3 (a) and the profile corresponding to a mean radius of 8″ (b). A helium line at $\sim 58\ \mathrm{km\ s}^{-1}$ is obvious in Fig. 3b. The value of y^+ inferred from this profile is 8.7 ± 1.9%, consistent with

Table 4. Ionized helium variations near component 3

Radius	H 76α					He 76α			y^+
	Cont.	Amp	V_{LSR}	ΔV	T_e^*	Amp	V_{LSR}	ΔV	
(arcsec)	(Jy)	(mJy)	($\mathrm{km\ s}^{-1}$)		(K)	(mJy)	($\mathrm{km\ s}^{-1}$)		(%)
8^+	0.7	28.9	60.9	33.8	18500	3.7	51	23	8.7
	(0.1)	(0.7)	(0.3)	(0.7)	(2700)	(0.5)	(2)	(4)	(1.9)
6.3	1.3	85.7	61.8	34.2	12600	7.1	55	19	4.6
	(0.2)	(1.7)	(0.3)	(0.8)	(2000)	(1.3)	(3)	(5)	(1.5)
5	0.9	60.2	61.2	24.7	12100	5.8	54	23	6.4
	(0.1)	(0.8)	(0.2)	(0.8)	(1400)	(0.6)	(2)	(3)	(1.1)
4.2	1.4	79.6	61.7	35.2	14000	6.3	56	20	4.5
	(0.2)	(1.3)	(0.2)	(0.6)	(2000)	(1)	(2)	(4)	(1.2)
2.9	1.4	88.4	61.4	38.6	11900	5.7	58	20	3.3
	(0.2)	(1.2)	(0.2)	(0.5)	(1700)	(1)	(2)	(4)	(0.9)
2.1[a]	1.8	131.0	61.8	40.5	10200	7.5	59	20	2.8
	(0.2)	(1.3)	(0.2)	(0.4)	(1100)	(1)	(2)	(4)	(0.7)
0	2.0	160.0	62.2	38.8	9700	9.5	58	17	2.6
	(0.2)	(1.5)	(0.2)	(0.6)	(1000)	(1.5)	(3)	(5)	(0.9)

[a] See Fig. 3

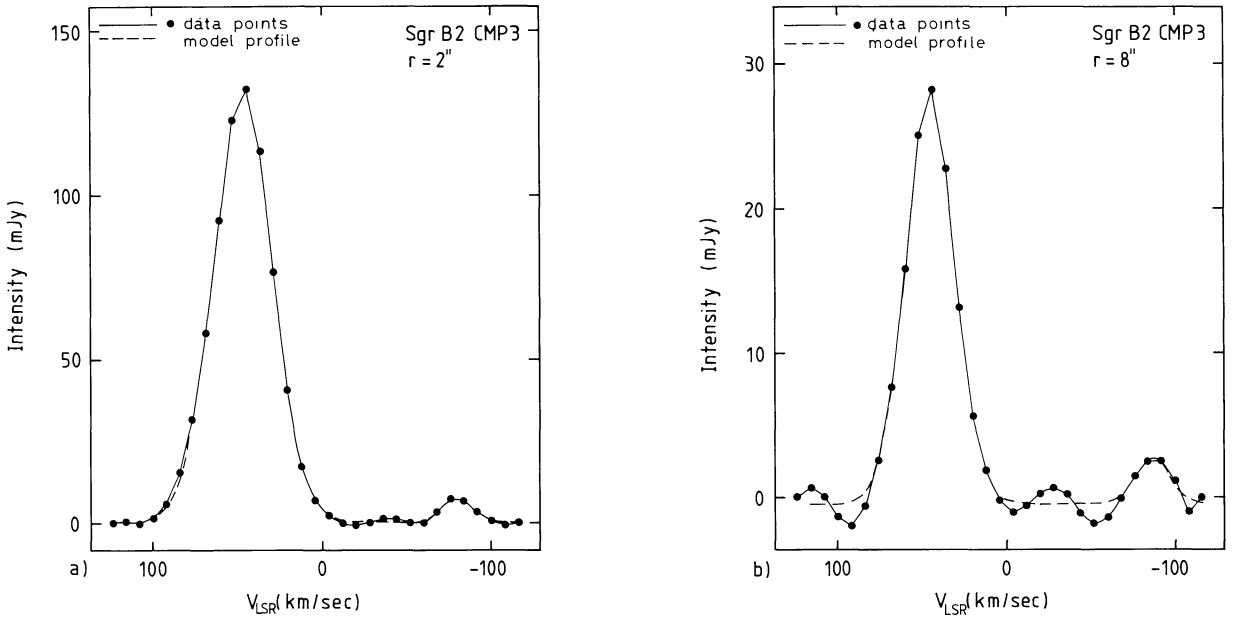

Fig. 3a and b. Line profiles illustrating the variations in apparent abundance of single ionized helium. **a** was obtained near the position of peak intensity of component 3 at $\alpha(1950) = 17^h44^m10^s.6$, $\delta(1950) = -28°22'03''$. **b** was obtained by integrating the line data over a ring of radius 8″ and width 2″ centred on the peak of component 3

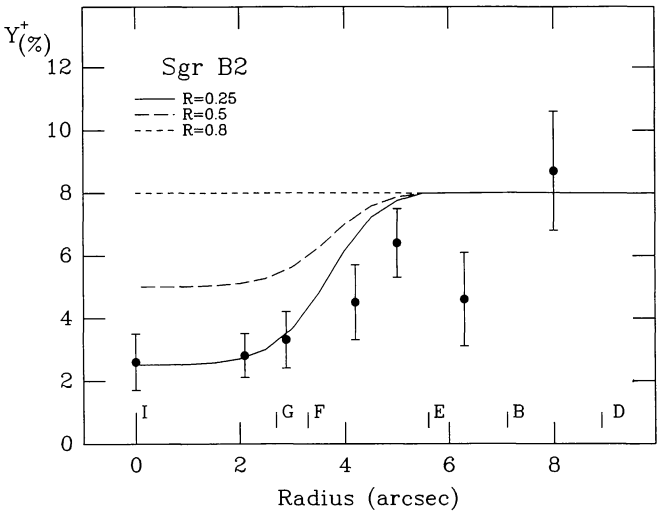

Fig. 4. Observed abundance of ionized helium (by number) as function of distance from the continuum peak of component 3 at $\alpha(1950) = 17^h44^m10^s.6$, $\delta(1950) = -28°22'03''$. The error bars indicate the formal $\pm 1\sigma$ errors. Note that these are lower limits to the actual local helium abundance. Also indicated are the positions of the continuum components B, D, E, F, and G (Benson and Johnston, 1984). The lines indicate y^+ as observed with 3″ resolution for various ratios (R) of the hydrogen to helium Strömgren radii in the compact components (see text)

y^+ as observed in the other components of Sgr B2. On the other hand profile (a) shows a significantly weaker helium line with a y^+ of only $2.8 \pm 0.7\,\%$. Over a range in radius of 8″ there is an increase in the apparent abundance of singly ionized helium of $5.9 \pm 2\,\%$. In Fig. 4 the variation of y^+ with radius is shown. The error bars indicate the $\pm 1\sigma$ error in each point. This figure clearly shows an increase of observed y^+ with distance from the centre of component 3. Also indicated are the radii at which the nearby compact components as identified by Benson and Johnston (1984) are located.

The four lines in Fig. 4 indicate theoretical values of the observed y^+ for various values of the ratio R of helium Strömgren radius (R_{He}) to hydrogen Strömgren radius (R_H) in the compact components. All models are based on the assumption of a true helium abundance (y^+_{true}) of 10 % and are calculated for a spatial resolution of 3″. The curves labelled $R = 0.25$, 0.5, and 0.8 indicate the observed y^+ if for component I (at the centre of component 3) such a ratio applies. For these three models components G, F, E, B, and D all have $R = 0.8$. Comparing these three curves with the observed points clearly shows that the observed variation in y^+ requires R in component I to be significantly less than 0.5. The LTE electron temperatures listed in Table 4 also show fairly large variations. As described in the previous section this is due to variations in continuum optical depth.

The question of the observed helium abundance in Sgr B2 has been hotly debated in the literature since 1973 (e.g. Churchwell and Mezger, 1973; Chaisson, 1973). Mezger (1980) reviewed the different mechanisms to explain observed abundances y^+ (from upper limits of only 2 %, e.g. Churchwell et al., 1974, to 8.5 %, Brown and Lockman, 1975) and concluded that, at least in most cases, the low observed abundances were due to what has become known as the geometric effect; the observed apparent abundance of ionized helium decreases with increasing beam size. Because the size of the observing beam depends on frequency, this effect appears as an increase of y^+ with increasing frequency. Other mechanisms to explain observed abundances (e.g. the "external maser effect", Brown and Gomez-Gonzales, 1975) could not satisfactorily explain the observed frequency dependance of y^+. The geometric effect can be understood if the region containing ionized helium is significantly different in size and/or shape from the region containing the ionized hydrogen. For such a region the observed y^+ is related to the true abundance y^+_{true} through a function depending on both the shape of the two regions and on the size of the observing beam. An obvious complication for most

single dish observations and even the current high resolution observations is the presence of more than one H II region in a single resolution element.

For the simple case of a spherically symmetric optically thin H II region observed with a gaussian beam Chaisson et al. (1978) derived such a relation between the observed quantity y^+ and the true abundance y^+_{true}. In the cases of low and high resolution this relation has the limiting forms:

$$y^+ = \frac{R_{He}^3}{R_H^3} * y^+_{true} \quad \text{(unresolved source)}$$

$$y^+ = \frac{R_{He}}{R_H} * y^+_{true} \quad \text{(resolved source).}$$

Thus in general the observed y^+ is a lower limit to y^+_{true}. It can be shown that such relations (under LTE conditions) are independent of the continuum optical depth τ_c and the relative location of the H and He ionized zones.

Several mechanisms to produce different Strömgren radii for H and He are possible. Firstly such a difference in R_H and R_{He} can occur if the ionizing source itself has a spectrum which contains relatively few He ionizing photons. This "mild" spectrum can come from either a cooler star ($T_{eff} < 35000$ K) or a star with an atmosphere which preferentially absorbs the He ionizing photons as compared to H ionizing photons e.g. through line blanketing (Mezger, 1980). Another possible cause is selective dust absorption (Mezger, 1980). In this model the dust inside the H II region preferentially absorps the He ionizing photons.

The observed low value of y^+ as shown in Fig. 4 implies that near component 3 there must be significant differences in the size of the H and He Strömgren spheres. From the total continuum flux density the number of Lyman continuum photons emitted by the ionizing source(s) can be calculated. For component 3, $N_{Lyc} \sim 8\ 10^{49}\ s^{-1}$, equivalent to one O4 star. On the other hand approximately 80 O9 stars (with $T_{eff} \sim 35000$ K) would be required to produce the same number of Lyman continuum photons. Such a large number of ionizing sources is very unlikely. Therefore cooler stars as the cause of $R_{He} < R_H$ can be ruled out; in component 3 selective absorbtion must be the cause of smaller values of y^+. At the centre of component 3 the emission observed within a single resolution element predominantly originates from an unresolved H II region in which a relatively large fraction of the He ionizing photons are absorbed. Thus at that position a low y^+ is measured. At positions away from the centre other H II regions are observed (also unresolved) in which less or no preferential absorbtion occurs. In these regions R_{He} approaches R_H resulting in an observed y^+ closer to y^+_{true}. The variation of y^+ with distance to the centre of component 3 thus must reflect a variation in the properties of either the dust inside the H II regions, or in the atmospheres of the ionizing stars. The relative smoothness of the changes in y^+ is caused by beam smearing (see Fig. 4). With sufficient resolution it should be possible to observe the individual H II regions in component 3 which have low values of y^+.

4.4. *G0.7N: components 7, 8, and 9*

G0.7N (components 7, 8, and 9, Benson and Johnston component K) forms a complex H II region. This complex has a continuum flux density which requires approximately four O5 stars for the excitation (see e.g. Benson and Johnston, 1984). The continuum structure (Fig. 5a) is complex showing two high intensity regions in the south (defined as components 7 and 8) and a lower intensity region north of those (component 9). These three components can also be identified in the 5 GHz map of Benson and Johnston (1984). The three components have different properties in the H 76α line. As can be seen in Table 3 the inferred electron temperatures (column 5) for all three components are in the range 6150 to 7000 K but the linewidths vary from 31.5 (component 7) to 48.2 km s^{-1} (component 9). Pressure broadening of the line in high density clumps can be ruled out because this would require a filling factor of $f \sim 10^{-4}$ which seems unlikely given the smooth appearance of the source as observed by Benson and Johnston (1984) with a resolution of 2.″7. Thus the line widths must be interpreted as due either to systematic motions within a single beam element or to turbulence in the ionized gas. Apart from the line widths the three components also have different central velocities. These differences are obvious in the velocity-right ascension plots at different declinations (see Fig. 6). The northern portion of G0.7N (component 9, Fig. 6a–c) has broad (up to $\Delta V = 50$ km s^{-1}) or even double profiles. In the southwest (component 7, Fig. 6d–g) the profiles are much narrower ($\Delta V \sim 30$ km s^{-1}) while in the southeast (component 8) again two broad ($\Delta V = 40$ km s^{-1}) components are observed. The southern half of the source clearly shows three distinct velocity components; at both the east and west edges a component at ~60–70 km s^{-1} and in the central region the velocity is more positive at ~80 km s^{-1} (Fig. 6d and e). In the northern part (component 9) the three components can still be observed; however here the velocity differences are less obvious because the lines are broader. The helium emission (in the right part of Fig. 6) shows the same trend in velocity. The H_2CO absorption lines as observed by Whieoak and Gardner (1986, in preparation) at 6 cm also show two velocity systems: one at 62 km s^{-1} and another at 80 km s^{-1}. These H_2CO velocity systems are indicated in Fig. 7a, e, and g.

In the lower panels of Fig. 5b and c the results of the gaussian analysis of the profiles in G0.7N are shown. The variations of line intensity (Fig. 5b) and velocity and line width (Fig. 5c) are shown. The similarity of the line intensity (Fig. 5b) distribution to the continuum (Fig. 5a) simply implies that the electron temperature is roughly constant at 6600 K over G0.7N. In contrast the line width (contours) and central velocity (gray scale) in Fig. 5c show that G0.7N has a multi-component structure in velocity. The positions with low line widths in the west have the higher central velocities and vice versa. The line widths range from 25 km s^{-1} (almost pure thermal broadening at an electron temperature of ~10000 K) to 55 km s^{-1}. Only in the extreme southern part of component 7 are the line widths as low as 25–30 km s^{-1}.

There are three possible explanations for these broad recombination lines in G0.7N: (1) turbulent motions up to 40 km s^{-1}, (2) blending of lines of two separate H II regions at different velocities, (3) or the presence of an expanding H II region which produces double peaked line profiles. Figure 7 provides some evidence in favour of one of the latter two solutions. Figure 7a shows a narrow line at $V_{LSR} = 80$ km s^{-1} with a halfwidth of 36 km s^{-1}. (The H 76α line also appears to have a low velocity wing, but a reliable two-component fit due to low signal to noise.) The profile shown in Fig. 7b was obtained one beamwidth to the east of the profile of Fig. 7a; a double peaked hydrogen line is observed in Fig. 7b with velocities at 55 and 88 km s^{-1}. Both an expanding shell as well as two separate regions in the line of sight at slightly different velocities would give rise to such profiles. Thus in this part of the source turbulent motions do not predominate. It is clear that higher resolution observations are required to decide which of these two possibilities is applicable.

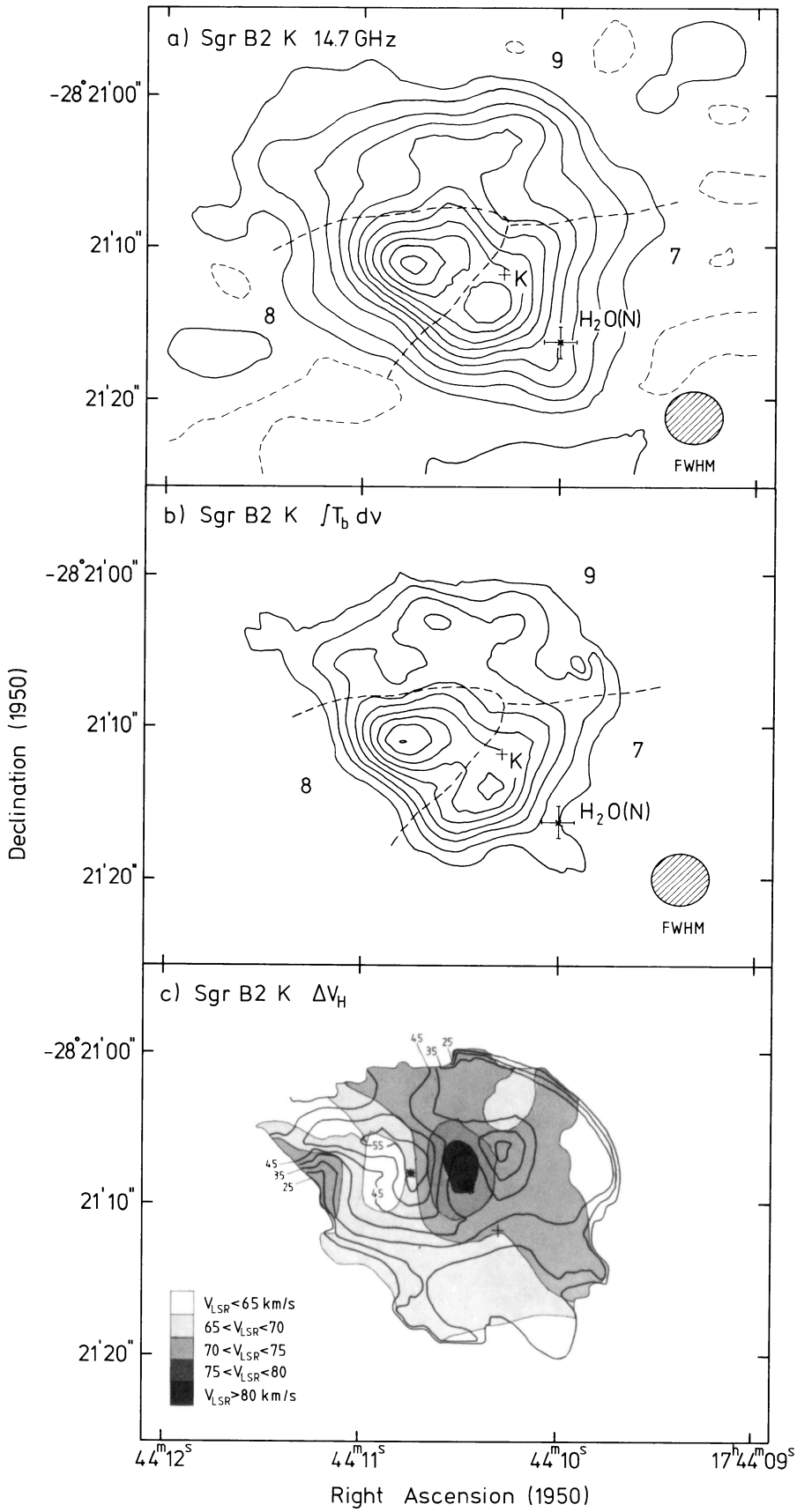

Fig. 5a–c. Components 7, 8, and 9. **a** Continuum brightness distribution at 14.7 GHz. The resolution in the map of $3''.8 \times 3''.4\,(\alpha \times \delta)$ is indicated by the shaded ellipse in the lower left corner. The division into the three components is indicated by the dashed lines. The cross indicates the position of component K as given by Benson and Johnson (1984). The position of the H_2O maser complex as found by Forster et al. (1978) is indicated as well. The contours are drawn at -25, 25, and 75 through 750 mJy beam^{-1} in 75 mJy beam^{-1} steps. The r.m.s. noise in the map is 13 mJy beam^{-1}. This map is not corrected for primary beam attenuation. **b** H 76α integrated line intensities obtained by fitting single gaussian profiles to individual spectra. The symbols have the same meaning as in Fig. 6a. The countour levels are at 500 through 4500 (mJy beam^{-1}) $\times$ (km s^{-1}) in steps of 500 (mJy beam^{-1}) $\times$ (km s^{-1}). The noise level is 250 (mJy beam^{-1}) $\times$ (km s^{-1}). The formal signal to noise ratio of the parameters of the fitted gaussians is greater than three at every point. **c** Linewidths (contours) and central velocities (gray levels) of the fitted single gaussian profiles. The contours are drawn at linewidths of 25 through 55 km s^{-1} with steps of 5 km s^{-1}. The central LSR velocities corresponding to the different gray levels are indicated in the lower left corner of the figure. The two stars mark the positions at which the line profiles shown in Fig. 7 were taken

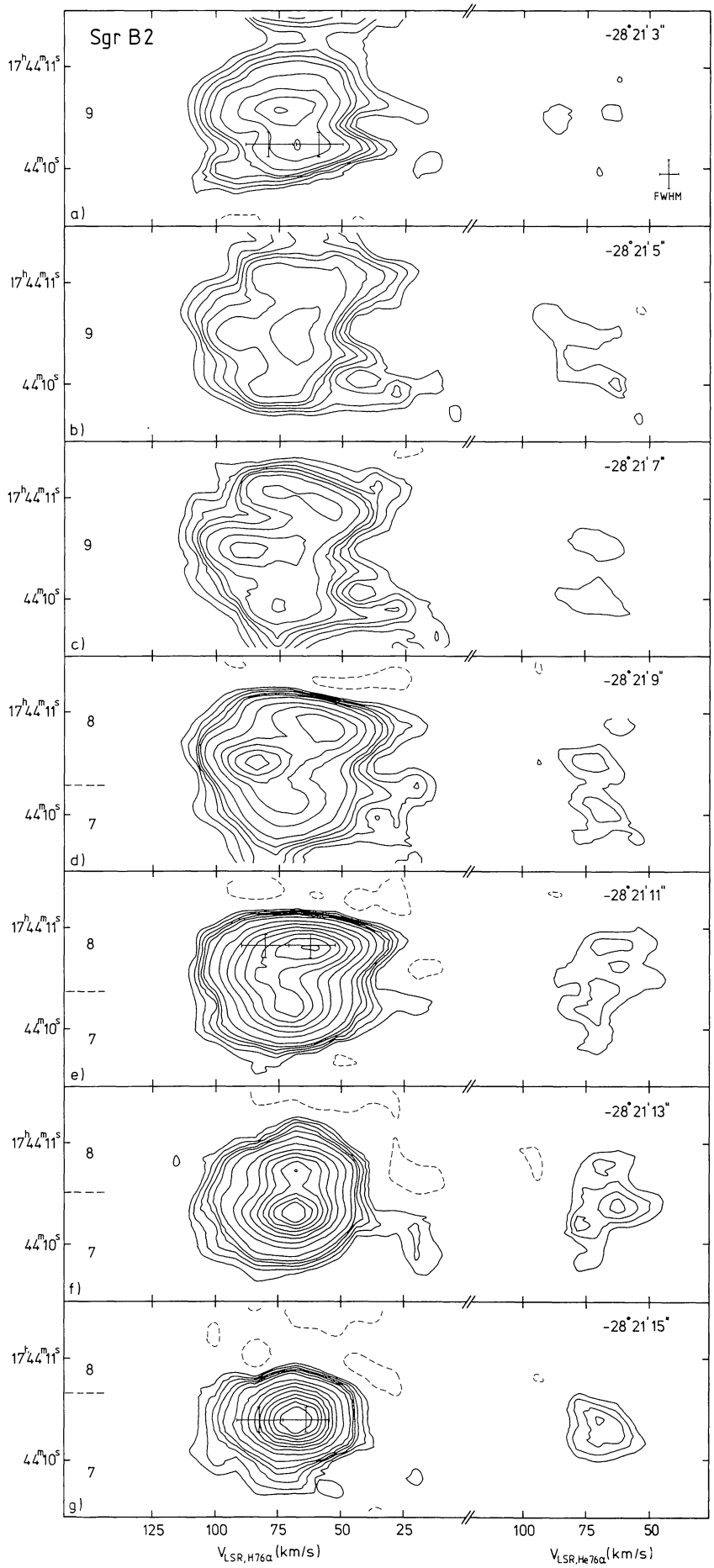

Fig. 6a–g. A mosaic of velocity-right ascention plots at different declinations in Sgr B2 components 7, 8, and 9. The declination of each map is indicated in the upper right corners. The boundary between components 7, 8, and 9 is at $\delta = -28°21'8''$. The boundary between components 7 and 8 is indicated in the lower panels. The H_2CO velocities as observed by Whiteoak and Gardner (in preparation) are indicated by the crosses in panels a, e and g. Note that there are two velocity scales: the left one for the H 76α and the right one for the He 76α emission. The contours are drawn at −5, 5, 7.5, 10, 12.5, 15, and 20 through 100 mJy beam^{-1} in 10 mJy beam^{-1} steps. The r.m.s. noise in these maps is 2.5 mJy beam^{-1}. The resolution ($3''.8 \times 8$ km s^{-1}) is indicated by the cross in the lower right corner of the upper panel

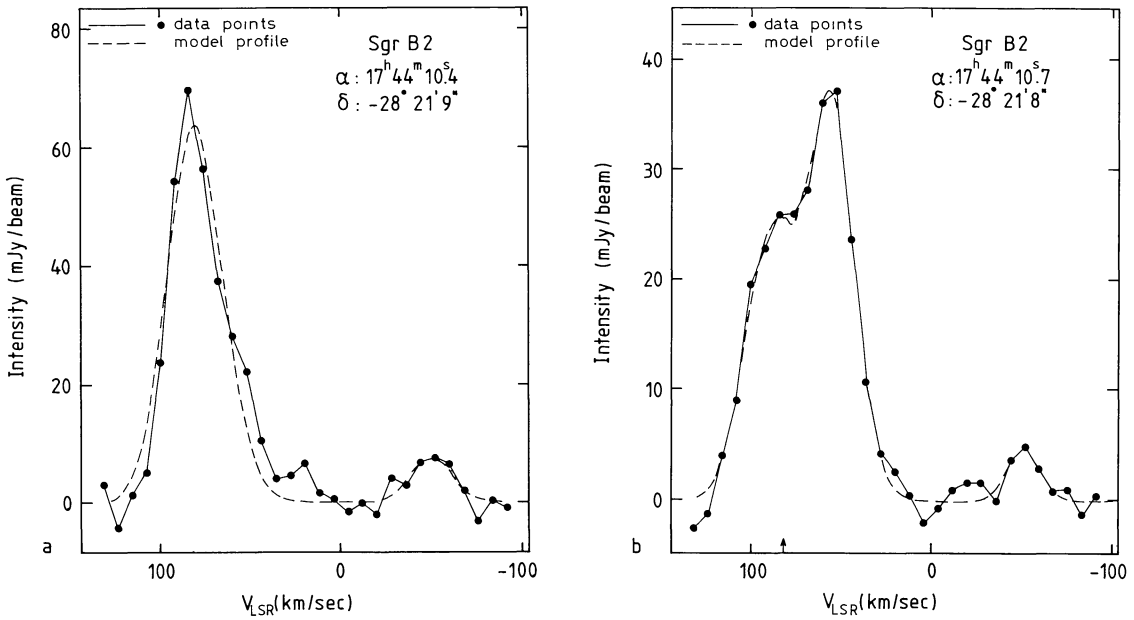

Fig. 7a and b. Two line profiles showing the great variations in line properties in Sgr B2 components 7, 8, and 9. The angular separation of the two profiles is 4″ or 0.2 pc (at 10 kpc). The positions are indicated in the top right corner of each profile. The full line indicates the observed profile, the dashed line a gaussian fit to the data. The H 76α velocity as derived from the profile in **a** is indicated by the arrow in the velocity scale of **b**

4.5. Conclusions

The H II complex Sgr B2 was mapped in the H 76α and He 76α recombination lines with high spatial resolution. Analysis of the line profiles of the 11 identified continuum components indicates that the abundance of singly ionized helium in this complex is 10%. This implies a helium abundance of at least 10% (by number) in Sgr B2.

Very low line to continuum ratios (2–3%) are observed towards the core of compact component 3. This is found to be due to the high continuum optical depth ($(\tau_c \sim 2)$.

A large variation of ionized helium abundance in the central region of Sgr B2 is found. This is most likely due to preferential absorption of He-ionizing photons in the atmosphere of the ionizing star of compact compact component 3 or by dust inside that component.

The H II complex G 0.7 N (components 7, 8, and 9) has at least three velocity systems, and probably consists of four or more compact H II regions. Double peaked line profiles suggest the presence of at least one expanding H II shell. Two of the identified velocity systems have counterparts in the molecular cloud surrounding the region.

Acknowledgements. We are greatful to C. Thum for the use of his data prior to publication. Roelfsema is supported by the Netherlands Foundation for Astronomical Research (ASTRON), which is financially supported by the Netherlands Organization for the Advancement of Pure Research (ZWO).

References

Allen, R.J., Ekers, R.D., Terlouw, J.P.: 1985, in *Proc. Intern. Workshop* on *Data Analysis in Astronomy* at Erice, eds. L. Scarci, V. di Gesu, Plenum, London
Benson, J.M., Johnston, K.J.: 1984, *Astrophys. J.* **277**, 181
Brown, R.L.: 1980, in *Proc. Workshop on Recombination Lines*, ed. P. Shaver, Reidel, Dordrecht
Brown, R.L., Gomez-Gonzales, J.: 1975, *Astrophys. J.* **200**, 598
Brown, R.L., Lockman, F.J.: 1975, *Astrophys. J.* **200**, L155
Chaisson, E.J.: 1973, *Astrophys. J.* **186**, 555
Chaisson, E.J., Lichten, S.M., Rodriguez, L.F.: 1978, *Astrophys. J.* **221**, 810
Churchwell, E., Mezger, P.G.: 1973, *Nature* **242**, 319
Churchwell, E., Mezger, P.G., Huchtmeier, W.: 1974, *Astron. Astrophys.* **32**, 283
Forster, J.R., Welch, W.J., Wright, M.C.H., Baudry, A.: 1978, *Astrophys. J.* **221**, 137
Garay, G., Reid, M.J., Moran, J.M.: 1985, *Astrophys. J.* **289**, 681
Garay, G.: 1985, in *Proc. ESO-IRAM-Onsala Workshop on (Sub)Millimeter Astronomy*, Aspenäs, Sweden, 17–20 June 1985, eds. P.A. Shaver, K. Kjär, *ESO Conf. Workshop Proc. No.* **22**, 517
Hobbs, R.W., Johnston, K.J.: 1971, *Astrophys. J.* **163**, 299
Högbom, J.A.: 1974, *Astron. Astrophys. Suppl.* **15**, 417
Mezger, P.G.: 1980, in *Proc. Workshop on Recombination Lines*, ed. P.A. Shaver, Reidel, Dordrecht
Mezger, P.G., Smith, L.F.: 1976, *Astron. Astrophys.* **61**, 715
Pitault, A., Cesarsky, D.A.: 1980, *Astron. Astrophys.* **82**, 203
Shaver, P.A.: 1980, *Astron. Astrophys.* **91**, 279
Thum, C., Mezger, P.G., Pankonin, V., Schraml, J.: 1978, *Astron. Astrophys.* **64**, L17